Draft version October 18, 2022
Typeset using LaTeX default style in AASTeX631

Inconspicuous Solar Polar Coronal X-ray Jets as the Source of Conspicuous *Hinode*/EUV Imaging Spectrometer (EIS) Doppler Outflows

Alphonse C. Sterling,[1] Conrad Schwanitz,[2,3] Louise K. Harra,[3,2] Nour E. Raouafi,[4] Navdeep K. Panesar,[5,6] and Ronald L. Moore[7,1]

[1] *NASA/Marshall Space Flight Center, Huntsville, AL 35812, USA*
[2] *Institute for Particle Physics and Astrophysics, ETH Zürich, 8092 Zürich, Switzerland*
[3] *Physikalisch Meteorologisches Observatorium Davos, World Radiation Center, 7260 Davos, Switzerland*
[4] *The John Hopkins University Applied Physics Laboratory, Laurel, MD 20723, USA*
[5] *Bay Area Environmental Research Institute, NASA Research Park, Moffett Field, CA 94035, USA*
[6] *Lockheed Martin Solar and Astrophysics Laboratory, 3251 Hanover Street, Building 252, Palo Alto, CA 94304, USA*
[7] *Center for Space Plasma and Aeronomic Research, University of Alabama in Huntsville, Huntsville, AL 35805, USA*

ABSTRACT

We examine in greater detail five events previously identified as being sources of strong transient coronal outflows in a solar polar region in *Hinode*/EUV Imaging Spectrometer (EIS) Doppler data. Although relatively compact or faint and inconspicuous in *Hinode*/Soft X-ray Telescope (XRT) soft-X-ray (SXR) images and in Solar Dynamics Observatory (*SDO*)/Atmospheric Imaging Assembly (AIA) EUV images, we find that all of these events are consistent with being faint coronal X-ray jets. The evidence for this is that the events result from eruption of minifilaments of projected sizes spanning 5000—14,000 km and with erupting velocities spanning 19—46 km s^{-1}, which are in the range of values observed in cases of confirmed X-ray polar coronal hole jets. In SXR images, and in some EUV images, all five events show base brightenings, and faint indications of a jet spire that (in four of five cases where determinable) moves away from the brightest base brightening; these properties are common to more obvious X-ray jets. For a comparatively low-latitude event, the minifilament erupts from near ($\lesssim$few arcsec) a location of near-eruption-time opposite-polarity magnetic-flux-patch convergence, which again is consistent with many observed coronal jets. Thus, although too faint to be identified as jets *a priori*, otherwise all five events are identical to typical coronal jets. This suggests that jets may be more numerous than recognized in previous studies, and might contribute substantially to solar wind outflow, and to the population of magnetic switchbacks observed in Parker Solar Probe (PSP) data.

Keywords: Solar filament eruptions, solar corona, solar x-ray emission, solar extreme ultraviolet emission

1. INTRODUCTION

Since the discovery of the solar wind it has been apparent that there is a nearly continuous outflow from the Sun. Recent observations from the Parker Solar Probe (*PSP*) (e.g. Bale et al. 2019) show that previously discovered magnetic disturbances in the solar wind magnetic field called *switchbacks* (e.g. Yamauchi et al. 2004) are extremely common. Exactly where the outflows, and features such as switchbacks, originate and how they are generated are outstanding puzzles.

Movies constructed from high-cadence images in lines sensitive to coronal emissions reveal a candidate source of those outflows and/or switchbacks, namely the transient outbursts known as *coronal jets*. These features take the form of long and narrow columns of emission at soft X-rays (SXR) and/or EUV wavelengths (Shibata et al. 1992; Cirtain et al. 2007). Observing in SXRs with the X-Ray Telescope (XRT) on the *Hinode* spacecraft, Savcheva et al. (2007) report that there are ∼60 jets/day in the two polar coronal holes. Assuming that jets are distributed evenly over the entire solar surface, taking the coronal holes to cover roughly 15% percent of the solar surface (Sheeley 1980; Harvey &

Recely 2002), and extrapolating to the entire Sun, gives only several hundred jets per hour, which is far from enough to explain the large quantities of switchbacks observed by PSP (e.g., Bale et al. 2019). If jets are a major source for switchbacks, and also perhaps of solar wind material, then they must be more frequent than the Savcheva et al. (2007) values.

Coronal outflows can also manifest in EUV spectral data, as blue shifts in spectral lines. Recently, Schwanitz et al. (2021) used data from the EUV Imaging Spectrometer (EIS) instrument on the *Hinode* spacecraft to look for such outflows. They found 14 outflow events in the data sets they examined (§2 provides more details on their data set).

Using this data set of EIS blueshifted events, Schwanitz et al. (2021) then performed an initial investigation of coronal EUV images, and also in SXR images for some events, to identify the source of the EIS blueshifts in those images. Among the entire set of 14 blueshifted events, they identified only five (events 1, 6, 11, 12, and 13 in their list) as corresponding to "obvious jets or bright points" in those images. And specifically, they identified only one of the 14, event 1 in their list (Table 1 in Schwanitz et al. 2021), as coinciding with an "obvious jet." This, therefore, implies that there might be frequent strong localized coronal outflows that occur in the low corona that are not due to features clearly identifiable as jets in the coronal images. This seemingly introduces a new puzzle, as to the cause of outflows if they are not jets.

In this paper, we will inspect more closely in coronal images a subset of the EIS blueshifted events of Schwanitz et al. (2021). Our subset consists of the first five of those events, labeled as events 1—5 in their paper. We will examine imaging data from SXRs and several EUV channels to see whether the source of these EIS blueshifted events can be identified with jets or jet-like features, when examined more extensively than in the Schwanitz et al. (2021) initial investigation. We limit our investigation to just the first five of their events because they are the only ones in the data set of 14 that include SXR data. By including the SXR data, we will be able to compare any possible jet signatures that we may find from the EIS blueshifted events more directly with earlier SXR-jet studies (e.g., Shibata et al. 1992; Shimojo et al. 1996; Cirtain et al. 2007; Savcheva et al. 2007; Sterling et al. 2015; Sterling et al. 2022). Also, jets that appear obvious in SXRs do not always manifest as obvious jet features in all EUV channels (Moore et al. 2010, 2013; Sterling et al. 2015; Sterling et al. 2022), and so by including both SXR and EUV images we will have a better chance of finding a jet corresponding to any of the five EIS Doppler events, if such a jet exists.

Central to our investigations will be our current understanding of how jets form. As noted above, the first detailed jet studies were with SXR observations. Among other findings, these observations revealed that jets have both a long spire that extends away from the surface, and a base region that is bright in SXRs. For many jets, the brightest portion of the bright base is localized in the base on one side of the spire (e.g., Shibata et al. 1992). Here we shall refer to this brightening as a "jet bright point" (JBP), following Sterling et al. (2015).

Observations in the EUV provided insight into the workings of many jets that are not readily apparent in SXR images alone. These wavelengths, at sufficient spatial and temporal resolution, show that many coronal jets result from eruptions of miniature filaments, or minifilaments (e.g., Nisticò et al. 2009; Moore et al. 2010, 2013; Shen et al. 2012; Adams et al. 2014). Based on observations of 20 jets in polar coronal holes, Sterling et al. (2015) argued that essentially all coronal jets result from minifilament eruptions, and they further argued that the JBP was actually a miniature flare, that forms below the erupting minifilament in a manner analogous to flares that occur below erupting large-scale filaments in typical solar eruptions. The jet-producing erupting minifilaments are essentially invisible in SXRs, which is why their importance was not recognized earlier.

Other studies have shown that the minifilaments erupt from miniature magnetic neutral lines, frequently where magnetic flux cancelation is occurring (e.g., Shen et al. 2012; Hong et al. 2014; Young & Muglach 2014a,b; Adams et al. 2014). A series of papers (Panesar et al. 2016, 2017, 2018a; McGlasson et al. 2019) shows that flux cancelation frequently accompanies jet production.

The schematic picture of Sterling et al. (2015) has been presented several times, and so it will not be repeated here (Fig. 1 of Sterling et al. 2018 gives a slightly updated version of the Sterling et al. 2015 schematic). Here we will describe the process assuming that the jet is occurring in a polar coronal hole's open-field. We use this assumption because (i) all of the jets of this paper occur in or around a polar coronal hole, and (ii) because assuming an open field simplifies the description somewhat. Actually however, the same basic process can hold for quiet Sun and active regions, but in those cases the field may be closed but far reaching instead of open. Jets are, in fact, also common in quiet Sun and even at the edge of active regions, and they likely operate in the fashion that we now describe.

Basically, the Sterling et al. (2015) picture says that polar coronal jets occur in regions of open magnetic field, where that field is rooted in flux of the hole's dominant magnetic polarity; for this discussion we will have the open-field

polarity be negative. The picture assumes (based on on-disk observations of jets, such as that of Adams et al. 2014) that an opposite-polarity (positive) magnetic flux element sits in this sea of negative flux. An "anemone" type of magnetic structure (Shibata et al. 2007) emanates from the positive patch in small loops from the positive element to the surrounding negative flux. This anemone structure is encased in negative-polarity open field, with the resulting structure having a magnetic null between the closed-field anemone and the open field above it. One side — appearing as a lobe in a 2-D cross-sectional cut — of the anemone develops a minifilament/flux rope on the neutral line between positive- and negative-polarity patches, while the other (larger-lobe) side of the anemone is nearly potential and does not have a minifilament. That minifilament/flux rope and its enveloping lobe field then erupt and move up along the outside of the potential-field lobe, until the erupting lobe field runs into oppositely directed open field on the far side of the potential-field lobe.

Two reconnections ensue during this minifilament eruption process: One is when the erupting lobe field enveloping the erupting minifilament/flux rope encounters the open field above the potential-field anemone lobe. This reconnection produces outflow of heated coronal plasma along the open field, forming a hot jet spire that is detected in SXRs and in some of the hotter EUV channels. Sterling et al. (2015) call this "external reconnection" (aka "interchange" or "breakout" reconnection), because it occurs external to the lobe field enveloping the erupting minifilament. A second reconnection, called "internal reconnection" occurs between the imploding legs of that erupting enveloping field. Sterling et al. (2015) argue that this internal reconnection results in the JBP, which corresponds to a typical solar flare that forms beneath an erupting typical-sized filament.

In followup studies to the Sterling et al. (2015) work, Panesar et al. (2016) and Panesar et al. (2017) argue that this minifilament/flux rope production and eruption result from magnetic flux cancelation along the neutral line, and that such cancelation first results in the formation of the minifilament, and that further cancelation leads to destabilization and eventual eruption of the minifilament to make the jet.

At least many jets are consistent with this "minifilament eruption" model, and with flux cancelation being responsible for the production and eruption of the minifilament/flux rope. For example, McGlasson et al. (2019) examined 60 on-disk coronal hole and quiet Sun jets, and found 85% of them resulted from minifilament eruptions that coincided closely in time to underlying flux cancelation. One study (Kumar et al. 2019) argues that actual flux cancelation is important only in a small percentage ($\sim$20%) of jets, with pre-jet field stressing by shearing and/or rotational photospheric motions playing a more important role. Another recent study however (Muglach 2021) also maintains that actual cancelation does coincide with most jets in that study. All of these studies are consistent with the minifilament-eruption picture and flux cancelation, or at least flux convergence and shearing, occurring for many jets in coronal holes and quiet Sun. Jets occurring at the periphery of active regions (e.g., Mulay et al. 2016; Sterling et al. 2016) may operate in the same way as described above for coronal hole and quiet Sun jets, but with somewhat different observational manifestations due to the stronger and more dynamic fields at those locations (Sterling et al. 2017). Numerical simulations recreate many of the aspects of this minifilament-eruption picture for producing jets (Wyper et al. 2017, 2018); those simulations emphasize the breakout reconnection (which we call the external reconnection above) in the formation of the jets, but the fundamental processes involved are as in the minifilament eruption picture of Sterling et al. (2015). Several reviews of coronal jets are available (e.g., Shimojo & Shibata 2000; Shibata & Magara 2011; Raouafi et al. 2016; Hinode Review Team et al. 2019; Innes et al. 2016; Sterling 2018; Shen 2021; Sterling 2021; Schmieder 2022).

In the following, we will examine EIS Doppler events 1 through 5 of Schwanitz et al. (2021). We will argue that the evidence indicates that each of these events originate from hard-to-detect jets that fit the minifilament-eruption picture for jets described above.

2. INSTRUMENTATION AND DATA

In this study we will use SXR images from *Hinode*/XRT (Golub et al. 2007), and EUV images from the Solar Dynamics Observatory (*SDO*)'s Atmospheric Imaging Assembly (AIA; Lemen et al. 2012). XRT is a grazing incidence X-ray telescope that observes the Sun using several broad-band filters. It has a detector of 512×512 square pixels, each $1\farcs02$ wide. Polar coronal jets, such as the features of relevance here, have been effectively viewed with XRT's filters sensitive to temperatures of $\gtrsim$1 MK (Cirtain et al. 2007), and this is fully consistent with measured temperatures of jet spires having values clustered in the 1.5—2.0 MK range (Pucci et al. 2013; Paraschiv et al. 2015). Here we use data obtained with XRT's "Al-Poly" filter, from a run of the *Hinode operations program* (HOP) 81. This HOP has been run on a regular basis since near the time of *Hinode*'s launch in 2006, and focuses observations on the solar polar

regions. The resulting images in our data set have an approximately 30 s cadence. XRT supports a variety of options for the field of view (FOV) of the images, and for these runs it was set to $384'' \times 384''$. For most of our analysis, and for most of the XRT images and movies presented here, we use cutouts of this full area to examine the features of interest more closely.

SDO/AIA routinely observes the entire solar disk in seven EUV filters. Here we examine in detail images from four filters, centered on wavelengths of He II 304, Fe IX 171, Fe XII 193, and Fe XV 211 Å. In contrast to the XRT Al-Poly filter, which is broadband and responsive to essentially all coronal temperatures in excess of ∼1 MK, AIA filters have a narrower temperature response; the 304, 171, 193, and 211 Å AIA filters to be used here are most sensitive to non-flaring coronal temperatures of approximately 50,000 K, 6×10^5 K, 1.5×10^6 K, and 2.0×10^6 K, respectively. We restrict ourselves to these four AIA filters because Sterling et al. (2015) found that the hotter-response AIA EUV channels (131, 335, and 94 Å) added little to the information obtainable from our four selected channels for the type of investigations to be done here in polar coronal hole regions.

We will be looking for faint features in the images, and we found it helpful to enhance them by performing a running sum over two successive images, while retaining the native cadences for the animations of the XRT and AIA images. We also enhance the contrast of weak features by taking the fourth root of the image intensities, before displaying them with the usual logarithmic scaling. We adjust the maximum and minimum intensity levels as needed for each event we examine to highlight features of interest. This same display technique was used in Sterling et al. (2022).

The events were originally selected by Schwanitz et al. (2021) from *Hinode*/EIS studies from three observation periods, consisting of 12 raster scans in total. Here we will look at the features from the first of these observation periods, during which this EIS study was also part of HOP 81. EIS took those scans on 2020 March 07, using the EIS 2″ slit and exposure times of 50 s, consisting of five rasters of duration 70 minutes each. Spectra were obtained in the Fe XII emission line at 195.12 Å, and were processed and fitted with single Gaussian profiles to obtain intensities and other information. Based on a rest wavelength, determined by using the average centroid of the entire raster, Schwanitz et al. (2021) marked times and locations that displayed blue shifts in excess of -6 km s^{-1}. In this fashion, they identified five EIS blue-shifted events in the coronal hole data over the chosen period, which are shown in Figure 1. (There were 14 such identifications in the full set of scans examined by Schwanitz et al. 2021.) The so-identified blue-shifted events were transient, in the sense that they did not exceed the duration of a single raster scan of 70 min, which was the finest time cadence available in that set of EIS data. Additionally, the blueshifted locations were localized; the largest blueshifted region among the five of the first scan was 3244 arcsec^2, and the other four at 721 arcsec^2 or less. Table 1 lists these five events, with the EIS time of observation (the time of the center of the blueshift contour) in column 1 and the blueshifted areas in column 2.

Figure 2 shows an XRT image of the north polar coronal hole region during the period of observation, at the time when event 3 is occurring. Also overplotted is a box showing the approximate FOV of the panel for this event in Figure 1. The accompanying animation shows the XRT observation over the entire period considered, with all five events examined here both labeled and including a box showing the FOV of the corresponding EIS panel in Figure 1. Table 1 gives in columns 3 and 4 the times and locations of the five events that we will inspect here in XRT and AIA images.

3. RESULTS

We consider each of the five EIS events, examining their XRT and AIA images in detail. We found all five of these events to be consistent with originating in the same fashion as typical coronal jets, namely via minifilament eruptions. We found, however, the arguments for this for cases events 3, 4, and 5 to be more straightforward than events 1 and 2. Therefore we will present our findings in that order.

3.1. *Event 3*

Event 3's probable source was described by Schwanitz et al. (2021) (in that paper's Table 1) as a "small-scale brightening." We will see that there is indeed a compact brightening that accompanies this outflow event. In the following, we argue that this is the brightening at the base of a faint, but otherwise typical, coronal jet.

Figure 3 shows our results for event 3. This is two six-panel arrays, with panels (a)—(f) showing the region around the event in different wavelength channels all at nearly the same time (within a few seconds), and panels (g)—(l) showing the same FOV of the same channels all at nearly the same time (again within a few seconds), but where the (g)-(l) times are about one minute later than the (a)—(f) panels. Each of the two sets shows images respectively in

AIA 171, 193, 211, and 304 Å in panels (a), (b), (d), and (e). Panels (c) and (f) show XRT images at the same time, with the image in panel (f) more zoomed-in than that in panel (c). Neither of the two XRT panels are as zoomed-in as the AIA panels, because we could not effectively zoom in as close with XRT due to its lower spatial resolution than AIA. An animation accompanying the on-line version shows the dynamic evolution of these panels over the course of event 3.

Figures 3(c) and 3(i) show XRT images close in time to Figure 2, so that the brightening pointed to by the blue arrows in the Figure 3 panels is identifiable in Figure 2, just above the "E3" label. In that larger FOV image of Figure 2 the feature seems nondescript. In Figure 3 however, we have zoomed in enough to see that there is an obvious eruption occurring at that location. Green arrows in Figures 3(a) and 3(g) point to this feature in 171 Å images, showing clear evolution over this one-minute time difference. The dynamic motion of this erupting feature is obvious in the accompanying animation, where the motion becomes apparent in 171 Å at 14:06:33 UT, and continues until the end of the animation at 14:34:45 UT. In the animation, the dynamic motion is apparent in the other three AIA channels as well.

We have measured the size of this erupting feature, using the 304 and 211 Å channel images at four different times between 14:08:21 and 14:09:05 UT, obtaining a size of $7\farcs8 \pm 0\farcs95$ for the mean and standard deviation of those four measurements. We also measured the speed of movement of the feature, using the same AIA channels and manually tracking different parts of the feature, over approximately 14:07:29 and 14:09:05 UT, giving 45.8 ± 15.4 km s^{-1} for the mean and standard deviation of those four measurements. All of these measurements are of the proper motion of the feature in projection against the observed solar disk.

The observed erupting feature in the AIA channels, as well as its lack of visibility in soft X-rays, are all consistent with the appearance of erupting minifilaments that produce coronal jets. Moreover, the measured length is within the range of the size measured for erupting minifilaments that made features that are unambiguously defined as polar coronal hole jets, albeit near the lower end of that range. Sterling et al. (2015) found for 18 such jets (out of their total set of 20 jets, with two of the events being too diffuse for adequate measurement) a size of $11'' \pm 7''$, and Sterling et al. (2022) found for an independent set of 20 soft X-ray polar coronal hole jets (out of 21 total jets) that the erupting minifilaments had size $14'' \pm 7''$. All of those measurements were made in a fashion similar to the method we use here; the specific AIA channel used for those measurements varied, but was among the same four channels used here. We believe that the differing channels is not a factor in the measurement in these cases however, because we selected a channel or channels where the cool-material erupting feature could be well seen. The AIA channel of best erupting-minifilament visibility varies from event to event, as discussed in some detail in Sterling et al. (2022).

Similarly, the speed that we find for for the erupting absorbing feature of event 3, $\sim$45 km s^{-1}, is similar to those that we measured for erupting minifilaments at the base of X-ray polar coronal hole jets in our previous studies: the 18 such jets of Sterling et al. (2015) had velocities of 31 ± 15 km s^{-1}; and while the 20 jets of Sterling et al. (2022) had average velocities and standard deviation of 26 ± 13 km s^{-1}, two of those jets had values in excess of 45 km s^{-1}. We have used the same general measurement techniques for the cool-material erupting features that we see here as we did in those two previous studies of the erupting minifilaments that we found at the base of the polar coronal hole jets. Because of the similarity in appearance, size, and velocity of the erupting feature causing event 3 to erupting minifilaments that we have identified previously, henceforth we will regard the dark feature that we see erupting in event 3 as an erupting minifilament.

Moreover, the brightening pointed to by the blue arrows in the Figure 3 XRT panels (c) and (i), and also visible as brightenings in panels of the AIA wavelengths, is similar to brightenings that we see at the base of erupting minifilaments. Comparison between the panels among the different wavelengths of the animation accompanying the figure also show that the erupting minifilament was originally seated near the solar surface at the location where the brightening later starts (at about 14:00 UT) in soft X-rays.

Because properties of the apparent erupting minifilament of event 3 are similar to erupting minifilaments that make confirmed jets, this similarity motivates the question of whether the event 3 erupting minifilament generated a coronal jet. The images and animation of Figure 3 argue that it does. White arrows in panels (h) and (i) show a feature that appears east of the location of the erupting minifilament. This feature is only weakly visible in the XRT images, but its structure persists for several frames in the animation. Similarly, the feature shows up well in the 193 Å AIA images. This feature is fully consistent with being the spire of a coronal jet. Moreover, the brightening pointed out by the blue arrows is then consistent with being a JBP typically seen accompanying coronal jets. In addition, the apparent spire moves with time over its life, consistent with what has been observed in jets (Shibata et al. 1992; Savcheva et al.

2007), and moreover, that movement with time is away from the location of the suspected JBP (Savcheva et al. 2007), and this is consistent with a jet resulting from the erupting minifilament (Baikie et al. 2022).

Figure 4, and its corresponding animation, show fixed-frame difference images of this event. Figure 4(a) reveals a feature that looks the same as a spire of typical coronal jets, and the animation shows that it moves away from the JBP just as in typical coronal jets. Therefore we conclude that our event 3 is indeed a faint version of a coronal jet.

Figure 4(b) shows a frame toward the end of the corresponding animation, with a region at the base showing a clear dimming signature. Such dimmings at coronal wavelengths can be indicative of showing locations where previously closed magnetic fields become temporarily open (e.g., Sterling & Hudson 1997; Zarro et al. 1999). Thus this dimming is consistent with material previously trapped near the solar surface escaping out along open field lines, which could account for the dimming signatures observed in EIS. From the non-differenced animation accompanying Figure 3, the erupting minifilament passes near the location of the dimming over about 14:08—14:10 UT, while dimming in the Figure 4 video is over primarily 14:10—14:20 UT; this supports that our observed dimming results from a field opening, rather than from a temporary obscuration of lower-height hot coronal material by cooler minifilament material passing above it. Thus our observed dimming accompanying our suspected jet of event 3 is a good candidate for being the source of the EIS outflows.

3.2. *Event 4*

Event 4's probable source was described by Schwanitz et al. (2021) (in that paper's Table 1) as a "small-scale eruption." Our work below will substantiate that assessment. We will further however argue that this small-scale eruption produces a weak (i.e., faint and comparatively hard-to-see) coronal jet.

Figure 5 shows our results for event 4. This again is two six-panel arrays, with the same layout as Figure 3. An animation accompanying the on-line version shows the dynamic evolution of these panels over the course of event 4.

We have again selected the AIA FOV to highlight a feature we observe near the time of event 4. In all four displayed AIA channels, this feature clearly appears to be an erupting minifilament. Arrows in panels (a) and (e) show it respectively in 171 and 304 Å images, and panels (g) and (k) show it having moved outward about four minutes later. As with event 3, we measure the mean length and speed of this feature, and find it to have size $17\farcs3 \pm 1\farcs5$, measured at three times in 304 Å images over the interval 14:09:53—14:15:17 UT. We find a mean speed projected against the solar disk from 304 Å images over 14:11:29—14:12:41 UT to be 29 ± 10 km s^{-1}. As with event 3, these values for the erupting cool material feature are within the ranges previously measured for X-ray-coronal-jet-producing minifilament eruptions. Thus, all indications are that this event-4 feature is equivalent to such an eruption.

Figures 5(i) and 5(l) show XRT frames with a very faint feature (white arrows), that appears to be consistent with a weak jet spire. Blue arrows in the same panels show a feature consistent with being a JBP accompanying the possible spire. From the animation accompanying that figure, that brightening is transient, appearing over about 14:13—14:29 UT. It occurs roughly in tandem with the prospective spire, and the prospective spire moves away from the brightening with time, over about 14:20—14:28 UT. All of this is consistent with the prospective spire again being a faint coronal jet spire, and the brightening being a typical JBP commonly occurring at the base of coronal jets. Returning to the AIA images, weakly enhanced intensity outflows consistent with this spire are discernible in 193 and 211 Å videos accompanying Figure 5, with the white arrows in Figure 5(h) pointing to the feature. From the videos, the outward movement of this feature has a large component of motion toward Earth. This likely is an additional factor in the extreme weakness of the spire in the images and videos. These observations support that this feature is a faint version of a coronal jet instigated by an erupting minifilament.

Clear apparent outflows are visible in the Figure 5 AIA 193 Å video over about 14:13—14:30 UT, leading to an intensity reduction (dimming) between the location of the brightening and the jet-spire feature pointed to by the arrows in Figure 5(h). Again, this dimming is consistent with being the source of the outflows recorded in the EIS Doppler spectral data.

These factors all support that event 4 is a faint coronal jet, and that it was the source of the corresponding EIS Doppler outflows.

3.3. *Event 5*

Event 5's probable source was described by Schwanitz et al. (2021) (in that paper's Table 1) as "unclear." We will argue here that the outflow is due to outflows along the spire of a coronal jet.

Figure 6 shows our results for event 5, with the same layout as Figures 3 and 5. An animation accompanying the on-line version shows the dynamic evolution of these panels over the course of event 5.

With the zoomed-in AIA images and animations, we again see clear evidence for an erupting minifilament in all four AIA channels. It might be best seen in 304 Å over 17:55—17:59 UT, crossing a bright feature. More generally, it is apparent in the 304 Å video over 17:53—18:00 UT. It is visible in the other AIA channels at the same time but with somewhat less contrast (with the scalings used here). We have measured the feature's length in 304 Å at three times over 17:56—-17:59 UT, obtaining $19\farcs3 \pm 0\farcs58$. For its speed projected against the disk, we used 304 Å images for three measurements over 17:55:05—17:57:53 UT, obtaining 32 ± 11 km s^{-1}. Again, these values are consistent with the feature being an erupting minifilament.

White arrows in Figure 6(l) point to either side of a spire-like feature. In the accompanying XRT video, there is clear evidence for a spire at that arrowed location starting shortly after the erupting minifilament occurs, expanding outward over 18:17—18:31 UT. Blue arrows in Figures 6(i) and 6(l) show a brightening with a burst of intensity over about 18:15—18:20 UT, in tandem with what looks like an opening up and expansion of the spire; this is consistent with being a jet-base JBP, with the jet spire again moving away from the JBP location (expanding away from the JBP over about 18:09—18:40 UT). A clear dimming signature is apparent in the XRT video over about 18:22—18:41 UT, occurring between the JBP and the spire location (the dark channel extending from the JBP at an angle to the north and slightly to the east at 18:41 UT was not present at 18:22 UT).

In this case, the apparent spire is rooted about $30''$ to the northeast of the brightening (Fig. 6(l). This is farther than the comparable distance in E3 (Fig. 3(i), where the separation is only a few arcsec), and in E4 (Fig. 5, where the separation is $\sim 5''$). Inspection of the AIA videos, however, shows that in this case there is a horizontal outflow that hugs the solar surface that originates near the minifilament-eruption location (where the JBP forms), out to near where the spire occurs. We show this movement with an arrow in the 171 Å video corresponding to Figure 6. The JBP in this case is well outside of the EIS box. One portion of that box is visible in the zoomed images of Figure 6, but we represent part of that box in frames (k) and (l) as blue lines; see the video accompanying Figure 2, which also includes those blue lines in the the XRT panel (during the first run of the video). Figure 6(l) shows that the spire occurs inside of the EIS outflow box, even though the JBP is outside of that box. Sterling et al. (2022), in Fig. 5 of that paper along with the accompanying animation, shows another example of substantial horizontal movement of an erupting minifilament, before the eruption turns outward to a spire some distance away from the JBP location.

It often is not possible to obtain useful line-of-sight HMI magnetic field information from polar-region features, because the photospheric fields detected by HMI are oriented primarily in the radial direction, meaning that the Earth-directed line-of-sight component is small with most of the true signal lost in the noise. We have found however that event 5 is at a low-enough latitude and that the region contains strong-enough fields for such magnetograms to be of qualitative use. Figure 7 shows these HMI magnetograms. Figure 7(a) shows contours from about the time of Figure 7(d), overlaid onto a grayscale version of a further-zoomed-in portion of the 304 Å image of Figure 6(e). There are two relatively strong opposite-polarity magnetic-flux patches very near the erupting-minifilament location. Reviewing the video accompanying Figure 6, it can be seen that the erupting minifilament erupts from a location near the neutral line of those flux patches, starting sometime before when the spire becomes discernible in the 304 Å images at about 17:54 UT. At that time it is about $3''$ away from that neutral line, and that is likely comparable to the alignment-offset uncertainty between the magnetograms and the AIA images. We can only say that the erupting minifilament originates from, and the JBP occurs at, a location close to the neutral line of that bipolar strong-flux patch.

Figure 7(b—d) show the evolution in time of this magnetic region, showing that the two flux patches approach each other in the hours prior to the minifilament eruption. As pointed out in §1, flux convergence and cancelation has been found to accompany jet onset closely in time in several studies of on-disk jets in quiet-Sun and coronal holes (Panesar et al. 2016, 2017, 2018a; McGlasson et al. 2019; Muglach 2021). And we have also observed similar flux cancelation at the time and base location of active-region jets (Sterling et al. 2016, 2017). In the present case, we see the patches approaching each other, and it is hard to confirm whether actual cancelation is occurring. Frequently such cancelation that apparently triggers the minifilament's eruption appears to be among "weak flux grains" near the neutral line of a larger-flux bipolar pair (Panesar et al. 2018a). If such cancelation is occurring in our event 5 case here, it would be beyond detectability in the line-of-sight magnetograms observing near the polar region. Therefore, we can only say that the convergence of the opposite-polarity bipolar pair that we observe here is consistent with flux cancelation triggering the eruption of the minifilament, as has been previously reported for more-on-disk coronal jets. Nonetheless, the behavior of the magnetic flux elements at the base of event 5 provides further evidence that it is a typical coronal jet, that is more faint than ones observed previously.

3.4. *Events 1 and 2*

We now consider events 1 and 2. These two EIS detections occurred at nearly the same location on the Sun, separated by about one hour in time. The probable sources were described as "obvious jets" for event 1 and as a "small-scale eruption" for event 2 by Schwanitz et al. (2021). Here we examine the features more closely.

From the video accompanying Figure 2, the two events appear to be in the same magnetically active location. In Figure 8 we show zoomed-in images, and accompanying videos, of the region encompassing both events.

3.4.1. *Event 1*

Figures 8(a—f) show event 1. We observe a jet-like spire in the XRT images, pointed to by the white arrow in Figure 8(f). From the accompanying video, the 304 Å images show an erupting cool-material feature. In this case, the feature is small and difficult to disentangle from the surrounding material. It still however looks similar to the erupting minifilaments that we detected in events 3—5. It is likely that this feature is less obvious than the erupting minifilaments of those previously examined events in part due to its proximity to the limb in this case, combined with its orientation, where we are viewing it looking nearly along its long axis. That is, it resembles the erupting minifilament of, say, event 4 viewed in 304 Å, but where we observe it viewing from the west (right) of the image in Figure 6(e). In the video accompanying Figure 8 we have followed the motion of the erupting cool feature with a black arrow, and it tracks closely in time and horizontal location the base of the spire of the jet feature in the XRT video. This spire feature is also apparent in AIA 193 and 211 Å videos. Furthermore, a brightening, consistent with being a JBP brightening, also occurs prominently in the XRT videos (and also in the AIA videos, with varying degrees of prominence depending on the channel) from very near the location from where the erupting cool-material feature emanated, and the spire feature moves away from the potential-JBP brightening. These characteristics between the erupting cool-material feature seen here, and the jet-like spire, and the brightenings at the base of the region from which the cool-material feature erupts, are all common to the majority of the cases we have examined of coronal jets resulting from erupting minifilaments that produce the jet spires and JBPs at the base location of those erupting minifilaments.

We have again measured the size and displacement speed of this erupting cool-material feature for event 1. From the 304 Å video, it is changing rapidly from frame to frame over the period when it is obvious and distinguishable from its surroundings, between 12:12:53 and 12:15:53 UT. We measured its size at the single time of 12:14:53 UT, and found it to be about 7″. We followed its displacement in 304 Å images over three different time period in the interval 12:12:41 and 12:15:41 UT, and found a speed of 19.6 ± 5.3 km s^{-1}. Although the size is on the small end, it is still within the ranges obtained in our earlier studies of erupting minifilaments that caused X-ray jets (with the values given in §3.1), and the speed is also well within the ranges of those previously measured values for such jets.

Because the quantitative properties of the erupting cool-material feature corresponding to event 1 are consistent with those of erupting minifilaments that produce X-ray jets, and because the morphological relationship of that erupting feature to the jet-like spire and base brightening resembles that of our previously observed jet-producing erupting minifilaments, we again conclude that the erupting cool-material feature is consistent with being an erupting minifilament that produces a coronal jet, and that the source of the EIS event 2 Doppler outflows is this coronal jet. Thus we support the Schwanitz et al. (2021) conclusion that the probable source of this outflow is a jet, and we have found that it operates in the same manner as other coronal jets that we have observed.

3.4.2. *Event 2*

Figures 8(g—l) show event 2. A white arrow points to a feature that appears to be a jet spire in the XRT image in 8(i), and the same feature is visible in 8(l). Also in Figure 8(i), a blue arrow points to a brightening that appears as a JBP at the base of that spire. From the animation corresponding to Figure 8, the apparent spire and JBP-like brightening show transient behavior typical of coronal jets, albeit substantially weaker than jets typically selected for jet analysis. In this case the intensity of the spire (faintly appearing over about 13:09 and 13:30 UT in the XRT animation, and pointed to by the white arrow in Fig. 8(i)) is too weak to confirm its movement toward, away from, or stationary relative to, the JBP location.

For this case, a corresponding feature in AIA images is less obvious than we found for the other events. Careful inspection however of the 171 Å images does show an absorption feature being ejected, which we indicate with the black arrow in 8(g). We track this feature with a black arrow in the animation corresponding to Figure 8. Its movement in the animation is closely in sync with the jet spire in the XRT panels. In addition to 171, this absorbing feature is also

faintly apparent in 193 and 211 Å animations. Thus this feature appears to be a cool-material erupting minifilament that accompanies the jet seen in the XRT images and animation, and which corresponds to the EIS outflows. In this case, the erupting minifilament is nearly lost in the coronal haze in the 171, 193, and 211 Å images.

No corresponding feature is discernible from the background in the 304 Å images and animations. This is not surprising, as this jet's spire in X-ray images remains narrow compared to the extent of that jet's base, and hence it would be classified as a "standard jet," in the terminology of Moore et al. (2010) and Moore et al. (2013), and those studies found that such standard jets often lack a significant corresponding jet spire in 304 Å images. (See Sterling et al. 2022 for further examples and further discussions on standard and blowout jets.)

In this case, it is likely that we are seeing the erupting minifilament at a different stage of its evolution than the other cases we have examined. Specifically, it looks as if this eruption is further underway by the time we can detect it, compared to other cases where the eruption seemed to be at its earliest stages. Therefore we do not include measurements of its size and speed of this feature for this event. Again, however, for this case also, this coronal jet is a candidate for being the source of the EIS Doppler outflows for event 2.

4. SUMMARY AND DISCUSSION

We have examined five locations in a polar coronal hole that displayed strong transient outflows of coronal material in *Hinode*/EIS Doppler images that were found by Schwanitz et al. (2021). They investigated 14 events in total, and here we concentrated on the first five events in their list, which were the ones with corresponding soft X-ray imaging data from *Hinode*/XRT. For our investigation here we primarily used XRT images, along with EUV images from *SDO*/AIA, to investigate in more detail the nature of the source regions for the outflows. Schwanitz et al. (2021) attributed the source of these five events to, respectively for events 1—5: "obvious jets," "small-scale eruption," "small-scale brightening," "small-scale eruption," and "unclear." Our closer examination here finds all five events to be consistent with being coronal X-ray jets. These jets are smaller-scale, fainter, and harder to detect than those in studies that specifically aimed at examining obvious jets. But upon close examination, the source locations for four of five of these events show quantitative and morphological similarities to the more-readily observed jets. The one remaining event, event 2, shows morphological similarities with more-readily observed jets, but it was too faint for us to obtain supporting quantitative measurements of its corresponding erupting minifilament's size and speed.

For all five events, we found dynamic absorbing features in the EUV images in the source regions identified by Schwanitz et al. (2021). For events 1, 3, 4, and 5, these outflowing events appeared extremely similar morphologically to the erupting minifilaments that we have observed numerous times at the base of clear coronal jets. Measurements of the erupting absorbing feature's length projected against the solar disk and their outward-moving speed values fell within the range that we had measured for the erupting minifilaments causing X-ray jets in polar coronal holes in our previous studies (Sterling et al. 2015; Sterling et al. 2022). Event 2 shows a similar erupting feature being expelled from the source region, although somewhat harder to see (likely due to obscuration by foreground material) and perhaps later in its eruption than for the other events. For each of these five events, further inspection of the soft X-ray XRT images and animations showed a spire-like feature, and a JBP-like brightening near the spire's base. Moreover, this spire moved away from the JBP in the four cases where the spire was bright enough to make a determination (all except for event 2). In addition, dimming signatures in events 3, 4, and 5, are consistent with material from the low corona being expelled in the jet episodes. (Candidates for similar dimmings exist in the events 1 and 2 XRT videos as well.) These morphological and measured characteristics are all consistent with the behavior of jets that fit the minifilament-eruption picture.

A common characteristic of jet-producing erupting minifilaments observed in on-disk jet events is that they originate from neutral lines between opposite-polarity flux patches, and furthermore, magnetic flux cancelation often occurs along that neutral line leading up to and during the time of the minifilament-eruption onset (e.g., Shen et al. 2012; Adams et al. 2014; Panesar et al. 2016, 2017, 2018a; Sterling et al. 2016, 2017; McGlasson et al. 2019; Muglach 2021). Although all of our events occur in a north polar coronal hole, one of these, event 5, is far enough south and has strong enough fields at its base for us to make some inferences about the erupting minifilament's magnetic environment. We find that the minifilament of the region indeed erupted within a few arcseconds of the neutral line of a bipolar pair of opposite-polarity magnetic patches. Moreover, in the hours prior to the minifilament's eruption and jet production, that pair of patches approached each other, consistent with flux cancelation being the cause of the minifilament's eruption. Thus these magnetic field observations are also consistent with the event 5 EIS outflow source region being a coronal jet.

One might ask: If the source of the strong EIS Doppler outflowing events are typical coronal jets, then why are those jets not more obvious as typical jets? In other words, why do we have to look at them with the deep analysis presented here before we can recognize them as coronal jets? There are two points to address in answering this: one is the nature of the typical jets of other studies compared with the jets identified in this study, and a second is why EIS happened to find the specific outflows examined in the Schwanitz et al. (2021) study.

Regarding the first point: A key difference between the jets found here and those found in other studies is that the other studies all started out specifically looking for jets. Thus, they examined jets that were comparatively easy to identify in images. The X-ray jets of Sterling et al. (2015) were ones that were well observed by Moore et al. (2013) in XRT images. Similarly, several other studies (Sterling et al. 2016, 2017; Sterling et al. 2022; Baikie et al. 2022) selected jets specifically because they were relatively well seen in XRT images. (Actually, Sterling et al. 2022 deliberately included a few jets that they described as "less prominent yet still distinct in XRT" in their study. Nonetheless those jets, which included J7, J8, J12, and J19 in their study, were still easier to identify in XRT images than the five jets of the present study.) All of those studies selected their jets by starting with movies formed from XRT images and specifically looking for jets. Similarly, there have been many studies of jets that began by looking for a set of jets in EUV movies (Nisticò et al. 2009; Panesar et al. 2016; Mulay et al. 2016; Panesar et al. 2017, 2018a; McGlasson et al. 2019; Kumar et al. 2019), and many additional studies looking at only about one or two jets, most of which began by looking for well-observed jets. Here, our approach was different, in that we did not specifically look for jets to study. Instead, interesting features with strong-outflow Doppler signatures in EIS spectral scans were first identified in the EIS observations, and then the solar coronal source for those regions were searched for in the EUV and SXR imaging data. What we found were disturbances that have the properties of coronal jets in the source regions, but those jet characteristics happen to be much harder to detect than in studies of jets found by specifically searching images for obvious jets.

Now on to the second point: The reason Schwanitz et al. (2021) only find outflows from jets that were comparatively weak and hard to detect is because EIS has a limited FOV and a low time cadence. The jet occurrence rate of about 30/day in a coronal hole deduced by Savcheva et al. (2007) is for jets that are relatively easy to see. From this we can expect about one such easy-to-see jet per hour in the entire coronal hole. Each EIS scan covers only $322'' \times 384''$, according to the information in the EIS study used for the observations (which was "*HOP81_new_study* with number 582," from Schwanitz et al. 2021), over about 70 minutes. The coronal hole studied by Savcheva et al. (2007) (see Cirtain et al. 2007) had about twice that extent in the east-west direction and so there is only a small chance that the $2''$-wide rastering EIS slit would pass over a substantial jet occurring about once an hour at a random location over the entire coronal hole and lasting only a few minutes. Thus EIS (operating in this mode) could easily miss a jet that would have been significant enough in X-ray images to be logged by studies specifically looking for such jets. Apparently instead, however, EIS found outflows from jets that were much less obvious (and likely more frequent) than those usually found in studies deliberately targeting X-ray jets.

These findings have significant implications for the occurrence frequency for outflow-producing coronal jets. The occurrence rates for jets of Savcheva et al. (2007), of ∼60/day in two polar coronal holes, relies upon jets that appeared as "visible ejection of material on a timescale of several tens of minutes" and that showed "a rapid increase in the length of [a jet-spire-like] brightness enhancement" with time. Thus, the jets they selected were, as would be expected from the above discourse, those that appeared clearly to be jets in XRT images. We have shown here that there are many features that are difficult to see in XRT images, but which are driven by the same processes that make the easier-to-see jets. Another factor is that several of the features we found were shrouded in quiet Sun "coronal haze." This factor alone could be largely responsible for the difficulty in identifying the jets.

Jets that appear in coronal holes unobscured by such haze are easier to see; this ease of visibility in coronal holes compared to quiet Sun was pointed out by Moore et al. (2013), and also discussed in Baikie et al. (2022). In addition to this being a consideration in the jet-count statistics of Savcheva et al. (2007), it also could explain why they found most of their jets to occur in polar coronal holes; even if jets exist in equal numbers in quiet Sun outside of those coronal hole regions, they may be harder to detect. A similar phenomenon was found with X-ray bright points (XBPs), which are X-ray-bright compact features mainly seen in polar coronal holes. Nakakubo & Hara (2000) found that XBP occurrence frequency seemingly is inversely related to the number of sunspots over a solar cycle, but they concluded that the apparent increase in XBPs during low-spot times was likely due to a decrease in the X-ray background intensity, rather than due to an actual increase in XBPs. Therefore, it is plausible that many coronal jets exist but are difficult to detect due to obscuration by foreground quiet-Sun coronal haze.

In addition, it is likely that there are many small-scale coronal jets that are difficult to detect in X-rays because they are intrinsically faint. Both of these factors could contribute to an underdetection of the true frequency of coronal jets in X-ray images, and also in EUV images. Revisiting the video accompanying Figure 2, it is apparent that only events 1 and 2 occur in a coronal-hole-appearing region. All of the other events either occur in quiet Sun, or perhaps in the polar coronal hole but with quiet-Sun corona in the foreground that partially obscures the event. This may explain why only event 1 was described as being due to "obvious jets" by Schwanitz et al. (2021). Event 2 also occurs in a coronal-hole-appearing location, but it was perhaps intrinsically too faint for a clear identification with a specific jet without the closer analysis performed here.

In addition to coronal jets observed in XRT images, there are smaller-scale jet-like features, called "jetlets" that appear at the base of polar plumes (Raouafi & Stenborg 2014). More generally, jetlets occur on the edges of the chromospheric network, and they may operate in the same manner as coronal jets (Panesar et al. 2018b; Panesar et al. 2019). Perhaps-similar features appear in active-region plage (Sterling et al. 2020a), and in ultra-high-resolution EUV images of features dubbed "campfires" (Panesar et al. 2021). On still smaller scales, there is the possibility that some fraction of spicules are produced in the same manner as coronal jets and jetlets, viz., via the minifilament-eruption mechanism operating on a much smaller size scale, via eruption of "microfilaments" (Sterling & Moore 2016; Sterling et al. 2020b).

If all of these jet-like features, including coronal jets, jetlets, and some fraction of spicules, operate in the same fashion as coronal jets, then it is possible that they all produce outflows similar to those detected from EIS, which here we argue are weak X-ray coronal jets. Then, in aggregate, these jet-like features resulting from small-scale eruptions might contribute substantially to the solar wind outflow. They may also contribute to the population of switchbacks that are observed in the solar wind observed by PSP (Horbury et al. 2020; Sterling et al. 2020b; Neugebauer & Sterling 2021), and even much earlier by Neugebauer (2012) based on observations of switchback-like phenomena in Ulysses data. Previously it had been suspected that coronal jets were not frequent enough to account for the large quantity of switchbacks observed by PSP. But it may be that the assumed number of jets is severely underestimated. To address the question directly will require development of methods to estimate the true rate of jet production. This requires estimating the effect of coronal haze on the counts, and further confirmation that the smaller-scale features, such as jetlets and spicules, are in fact due to eruption of small-scale filament-like features, triggered to erupt by magnetic flux cancelation at their bases.

It is also desirable to observe spectroscopically, with spectral scans such as those done with EIS by Schwanitz et al. (2021), a bone fide "typical" coronal jet. It would be of interest to see whether such a jet results in outflows similar to those of the Schwanitz et al. (2021) events, except perhaps stronger (which might be evidenced by a stronger emission-measure depletion, for example). Such observations could provide additional support that Schwanitz et al. (2021) features, at least the five examined here, are indeed small-scale version of such bona fide coronal jets. It will also be of interest to see how the outflows here connect to other outflow events commonly observed with EIS and similar spectrometers (e.g. Harra et al. 2008; Brooks & Warren 2011; Harra et al. 2012; Brooks et al. 2020; Tian et al. 2021; Yardley et al. 2021). It is also of interest to investigate whether the EIS Doppler features referred to as dark jets by Young (2015) might be similar to the features we observe here.

A.C.S., R.L.M. and N.K.P. received funding from the Heliophysics Division of NASA's Science Mission Directorate through the Heliophysics Supporting Research (HSR, grant No. 20-HSR20_2-0124) Program, and the Heliophysics Guest Investigators program. A.C.S. and R.L.M. also received support from the Heliophysics System Observatory Connect (HSOC, grant No. 80NSSC20K1285) Program. A.C.S. received additional support through the MSFC *Hinode* Project, and N.K.P. received additional support through a NASA *SDO*/AIA grant. *Hinode* is a Japanese mission developed and launched by ISAS/JAXA, with NAOJ as domestic partner and NASA and UKSA as international partners. It is operated by these agencies in co-operation with ESA and NSC (Norway). We acknowledge the use of AIA data. AIA is an instrument onboard *SDO*, a mission of NASA's Living With a Star program.

REFERENCES

Adams, M., Sterling, A. C., Moore, R. L., & Gary, G. A. 2014, Astrophysical Journal, 783, 11, doi: 10.1088/0004-637X/783/1/11

Baikie, T. K., Sterling, A. C., Moore, R. L., et al. 2022, arXiv e-prints, arXiv:2201.08882. https://arxiv.org/abs/2201.08882

Bale, S. D., Badman, S. T., Bonnell, J. W., et al. 2019, Nature, 576, 237, doi: 10.1038/s41586-019-1818-7

Brooks, D. H., & Warren, H. P. 2011, ApJL, 727, L13, doi: 10.1088/2041-8205/727/1/L13

Brooks, D. H., Winebarger, A. R., Savage, S., et al. 2020, ApJ, 894, 144, doi: 10.3847/1538-4357/ab8a4c

Cirtain, J. W., Golub, L., Lundquist, L., et al. 2007, Science, 318, 1580, doi: 10.1126/science.1147050

Golub, L., Deluca, E., Austin, G., et al. 2007, Solar Physics, 243, 63, doi: 10.1007/s11207-007-0182-1

Harra, L. K., Archontis, V., Pedram, E., et al. 2012, SoPh, 278, 47, doi: 10.1007/s11207-011-9855-x

Harra, L. K., Sakao, T., Mandrini, C. H., et al. 2008, ApJL, 676, L147, doi: 10.1086/587485

Harvey, K. L., & Recely, F. 2002, SoPh, 211, 31, doi: 10.1023/A:1022469023581

Hinode Review Team, Khalid, A.-J., Patrick, A., et al. 2019, Publications of the Astronomical Society of Japan, 71, id.R1, doi: 10.1093/pasj/psz084

Hong, J., Jiang, Y., Yang, J., et al. 2014, Astrophysical Journal, 796, 73, doi: 10.1088/0004-637X/796/2/73

Horbury, T. S., Woolley, T., Laker, R., et al. 2020, Astrophysical Journal Supplement Series, 246, 45, doi: 10.3847/1538-4365/ab5b15

Innes, D. E., Bučík, R., Guo, L. J., & Nitta, N. 2016, Astronomische Nachrichten, 337, 1024, doi: 10.1002/asna.201612428

Kumar, P., Karpen, J. T., Antiochos, S. K., et al. 2019, Astrophysical Journal, 873, 93, doi: 10.3847/1538-4357/ab04af

Lemen, J. R., Title, A. M., Akin, D. J., et al. 2012, Solar Physics, 275, 17, doi: 10.1007/s11207-011-9776-8

McGlasson, R. A., Panesar, N. K., Sterling, A. C., & Moore, R. L. 2019, ApJ, 882, 16, doi: 10.3847/1538-4357/ab2fe3

Moore, R. L., Cirtain, J. W., Sterling, A. C., & Falconer, D. A. 2010, Astrophysical Journal, 720, 757, doi: 10.1088/0004-637X/720/1/757

Moore, R. L., Sterling, A. C., Falconer, D. A., & Robe, D. 2013, Astrophysical Journal, 769, 134, doi: 10.1088/0004-637X/769/2/134

Muglach, K. 2021, ApJ, 909, 133, doi: 10.3847/1538-4357/abd5ad

Mulay, S. M., Tripathi, D. T., Del Zanna, G., & Mason, H. 2016, Astronomy and Astrophysics, 589, A79, doi: 10.1051/0004-6361/201527473

Nakakubo, K., & Hara, H. 2000, Advances in Space Research, 25, 1905, doi: 10.1016/S0273-1177(99)00621-3

Neugebauer, M. 2012, ApJ, 750, 50, doi: 10.1088/0004-637X/750/1/50

Neugebauer, M., & Sterling, A. C. 2021, ApJL, 920, L31, doi: 10.3847/2041-8213/ac2945

Nisticò, G., Bothmer, V., Patsourakos, S., & Zimbardo, G. 2009, Solar Physics, 259, 87, doi: 10.1007/s11207-009-9424-8

Panesar, N. K., Sterling, A. C., & Moore, R. L. 2017, Astrophysical Journal, 844, 131, doi: 10.3847/1538-4357/aa7b77

—. 2018a, Astrophysical Journal, 853, 189, doi: 10.3847/1538-4357/aaa3e9

Panesar, N. K., Sterling, A. C., Moore, R. L., & Chakrapani, P. 2016, Astrophysical Journal, 832L, 7, doi: 10.3847/2041-8205/832/1/L7

Panesar, N. K., Sterling, A. C., Moore, R. L., et al. 2018b, Astrophysical Journal, 868L, 27, doi: 10.3847/2041-8213/aaef37

Panesar, N. K., Tiwari, S. K., Berghmans, D., et al. 2021, ApJL, 921, L20, doi: 10.3847/2041-8213/ac3007

Panesar, N. K., Sterling, A. C., Moore, R. L., et al. 2019, ApJL, 887, L8, doi: 10.3847/2041-8213/ab594a

Paraschiv, A. R., Bemporad, A., & Sterling, A. C. 2015, A statistical study with Hinode XRT data, Astronomy and Astrophysics, 579, 96, doi: 10.1051/0004-6361/201525671

Pucci, S., Poletto, G., Sterling, A. C., & Romoli, M. 2013, Astrophysical Journal, 776, 16, doi: 10.1088/0004-637X/776/1/16

Raouafi, N. E., & Stenborg, G. 2014, Astrophysical Journal, 787, 118, doi: 10.1088/0004-637X/787/2/118

Raouafi, N. E., Patsourakos, S., Pariat, E., et al. 2016, Space Science Reviews, 201, 1, doi: 10.1007/s11214-016-0260-5

Savcheva, A., Cirtain, J., Deluca, E. E., et al. 2007, Publications of the Astronomical Society of Japan, 59, 771, doi: 10.1093/pasj/59.sp3.S771

Schmieder, B. 2022, arXiv e-prints, arXiv:2201.11541. https://arxiv.org/abs/2201.11541

Schwanitz, C., Harra, L., Raouafi, N. E., et al. 2021, SoPh, 296, 175, doi: 10.1007/s11207-021-01915-0

Sheeley, N. R., J. 1980, SoPh, 65, 229, doi: 10.1007/BF00152791

Shen, Y. 2021, Proceedings of the Royal Society of London Series A, 477, 217, doi: 10.1098/rspa.2020.0217

Shen, Y., Liu, Y., Su, J., & Deng, Y. 2012, Astrophysical Journal, 745, 164, doi: 10.1088/0004-637X/745/2/164

Shibata, K., & Magara, T. 2011, LRSP, 8, 6

Shibata, K., Ishido, Y., Acton, L. W., et al. 1992, Publications of the Astronomical Society of Japan, 44, L173

Shibata, K., Nakamura, T., Matsumoto, T., et al. 2007, Science, 318, 1591, doi: 10.1126/science.1146708

Shimojo, M., Hashimoto, S., Shibata, K., et al. 1996, Publications of the Astronomical Society of Japan, 48, 123, doi: 10.1093/pasj/48.1.123

Shimojo, M., & Shibata, K. 2000, Astrophysical Journal, 542, 1100, doi: 10.1086/317024

Sterling, A. C. 2018, in Journal of Physics Conference Series, Vol. 1100, Journal of Physics Conference Series, 012024, doi: 10.1088/1742-6596/1100/1/012024

Sterling, A. C. 2021, in Solar Physics and Solar Wind, ed. N. E. Raouafi & A. Vourlidas, Vol. 1, 221, doi: 10.1002/9781119815600.ch6

Sterling, A. C., & Hudson, H. S. 1997, ApJL, 491, L55, doi: 10.1086/311043

Sterling, A. C., & Moore, R. L. 2016, Astrophysical Journal, 828, L9, doi: 10.3847/2041-8205/828/1/L9

Sterling, A. C., Moore, R. L., Falconer, D. A., & Adams, M. 2015, Nature, 523, 437, doi: 10.1038/nature14556

Sterling, A. C., Moore, R. L., Falconer, D. A., et al. 2016, Astrophysical Journal, 821, 100, doi: 10.3847/0004-637X/821/2/100

Sterling, A. C., Moore, R. L., Falconer, D. A., Panesar, N. K., & Martinez, F. 2017, Astrophysical Journal, 844, 28, doi: 10.3847/1538-4357/aa7945

Sterling, A. C., Moore, R. L., & Panesar, N. K. 2018, Astrophysical Journal, 864, 68, doi: 10.3847/1538-4357/aad550

Sterling, A. C., Moore, R. L., & Panesar, N. K. 2022, ApJ, 927, 127, doi: 10.3847/1538-4357/ac473f

Sterling, A. C., Moore, R. L., Panesar, N. K., et al. 2020a, ApJ, 889, 187, doi: 10.3847/1538-4357/ab5dcc

Sterling, A. C., Moore, R. L., Samanta, T., & Yurchyshyn, V. 2020b, ApJL, 893, L45, doi: 10.3847/2041-8213/ab86a5

Tian, H., Harra, L., Baker, D., Brooks, D. H., & Xia, L. 2021, SoPh, 296, 47, doi: 10.1007/s11207-021-01792-7

Wyper, P. F., Antiochos, S. K., & DeVore, C. R. 2017, Nature, 544, 452, doi: 10.1038/nature22050

Wyper, P. F., DeVore, C. R., & Antiochos, S. K. 2018, Astrophysical Journal, 852, 98, doi: 10.3847/1538-4357/aa9ffc

Yamauchi, Y., Suess, S. T., Steinberg, J. T., & Sakurai, T. 2004, Journal of Geophysical Research: Space Physics, 109, A03104, doi: 10.1029/2003JA010274

Yardley, S. L., Brooks, D. H., & Baker, D. 2021, A&A, 650, L10, doi: 10.1051/0004-6361/202141131

Young, P. R. 2015, ApJ, 801, 124, doi: 10.1088/0004-637X/801/2/124

Young, P. R., & Muglach, K. 2014a, Solar Physics, 289, 3313, doi: 10.1007/s11207-014-0484-z

—. 2014b, Publications of the Astronomical Society of Japan, 66, 12, doi: 10.1093/pasj/psu088

Zarro, D. M., Sterling, A. C., Thompson, B. J., Hudson, H. S., & Nitta, N. 1999, ApJL, 520, L139, doi: 10.1086/312150

Table 1. EIS Outflow Events Observed with XRT and AIA

Event	EIS Time (UT)[a]	EIS Size (arcsec^2)[a]	XRT Time (UT)[b]	XRT Location[b]	EMF Size (km)[c]	EMF Velocity (km s^{-1})[c]	EMF Notes[d]
1	12:17:55	3244	12:14—12:29	(-100,900)	≈5000	19.6 ± 5.3	Small-sized EMF visible in 304 Å.
2	13:18:39	677	13:09—13:22	(-60,900)	Uncertain	Uncertain	Strands of an EMF visible in 171 Å.
3	14:09:00	245	14:00 —14:14	(30,860)	5700 ± 690	46 ± 15	EMF visible in all channels. Confined eruption.
4	14:28:34	721	14:14—14:32	(-70,720)	$12{,}600 \pm 110$	29 ± 10	Clear EMF in all channels, maybe best in 304 Å.
5	18:32:16	365	18:00—18:45+	(-199,800)	$14{,}000 \pm 420$	32 ± 11	Clear EMF in all channels, maybe best in 304 Å. Appears to be ejective.

[a] From Table 2 of Schwanitz et al. (2021).

[b] XRT jet times and locations, in arcseconds from disk center. Locations are approximate, based on video in Fig. 2 (which is rotated to 2020 March 7, 15:00 UT).

[c] Size and velocity of erupting minifilament (EMF) from AIA images, with 1σ standard deviations where determined (see text for details).

[d] Notes on detectability of EMF in AIA images.

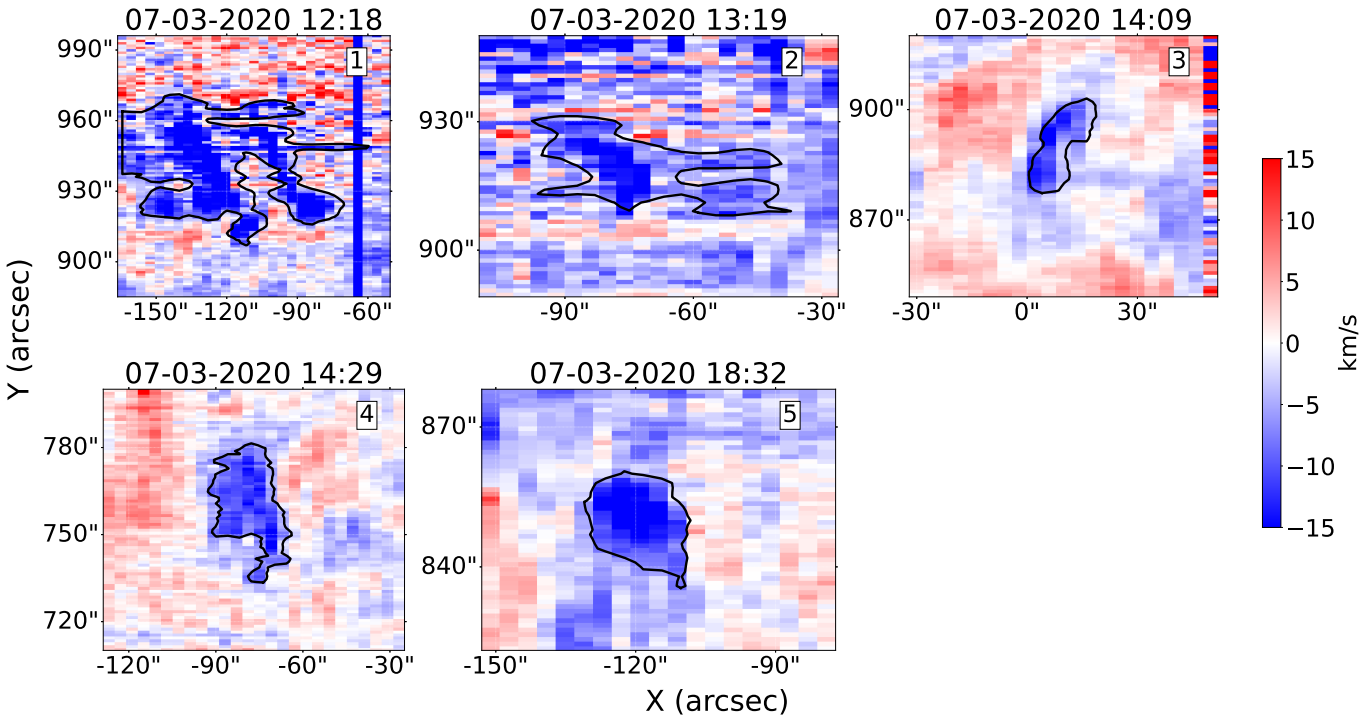

Figure 1. EIS-observed Doppler outflow events for the five events studied here, in the Fe XII 195.12 Å emission line. These are the first five events studied in Schwanitz et al. (2021), with the event number (which also corresponds to the event numbers of this paper) given in the upper right of each panel, and with each event's date and time of the center of the Doppler outflow observations given at the top of each panel in DD-MM-YYYY HH:MM format. Deep blue features inside the contours represent observed outflows in excess of Doppler velocity $-6\,\mathrm{km\ s^{-1}}$. See §2 and Schwanitz et al. (2021) for other details.

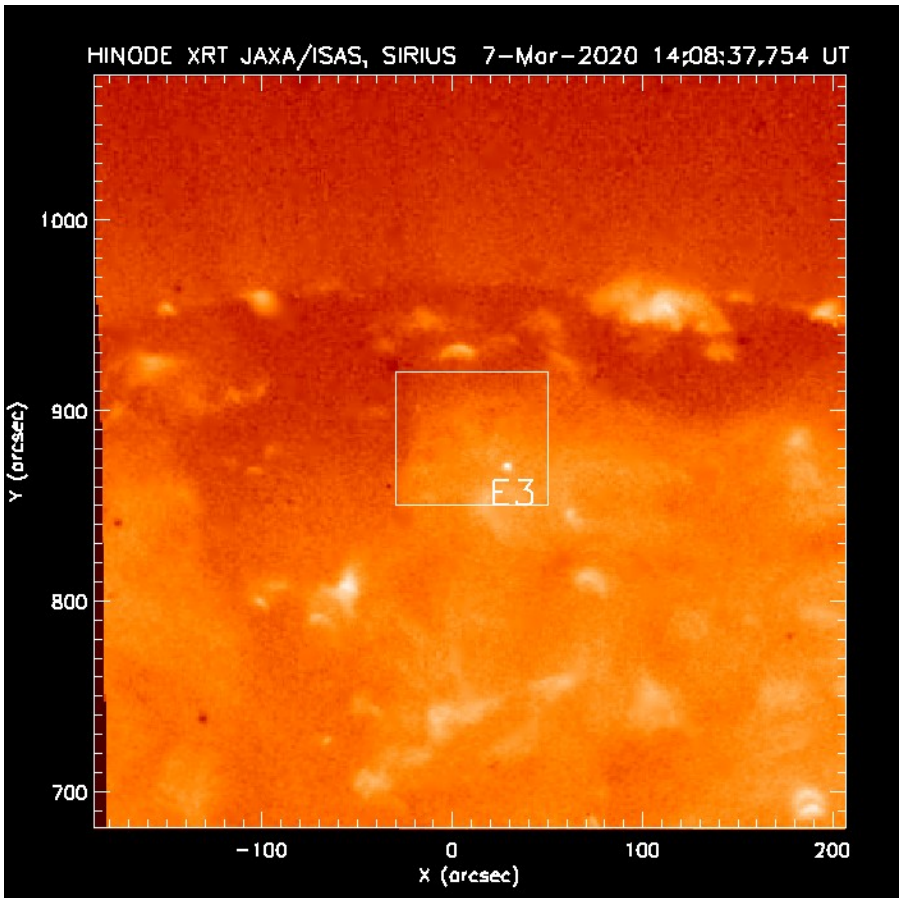

Figure 2. A soft X-ray image from the *Hinode* XRT instrument's Al Poly filter, of the north polar coronal hole region on 2020 March 7, showing an overview of the northern polar coronal hole region where all of the events studied here occurred. One of the events of Table 1, labeled E3, is in progress, and the white box shows the approximate field of view displayed for the corresponding EIS-outflow event in Fig. 1. North is up and west is to the right in this and in all other solar images and animations of this paper. Dark spots in the image, e.g. at (-140,740), and similar patches and blotches, are artifacts. The accompanying animation shows the XRT movie for this period, covering 2020 March 7 over 12:00:01—18:45:20 UT, but with a gap between 14:34:46 and 16:30:15 UT because there are no events in our data set over that interval. That animation contains labels and boxes similar to those shown for event 3 in this figure, but for all five events, with the coordinates of the boxes in Fig. 1 giving the approximate locations of those boxes for each respective jet in the movie. In that animation at the time of event 5, the "E5" label is located near a brightening that is the suspected source region of the outflows, which is located about 30″ south of the EIS box showing the EIS Fig. 1 panel's FOV; see §3.3 for discussion of the spire and observed EIS outflows being separated from the brightening. The entire movie runs for 26 s.

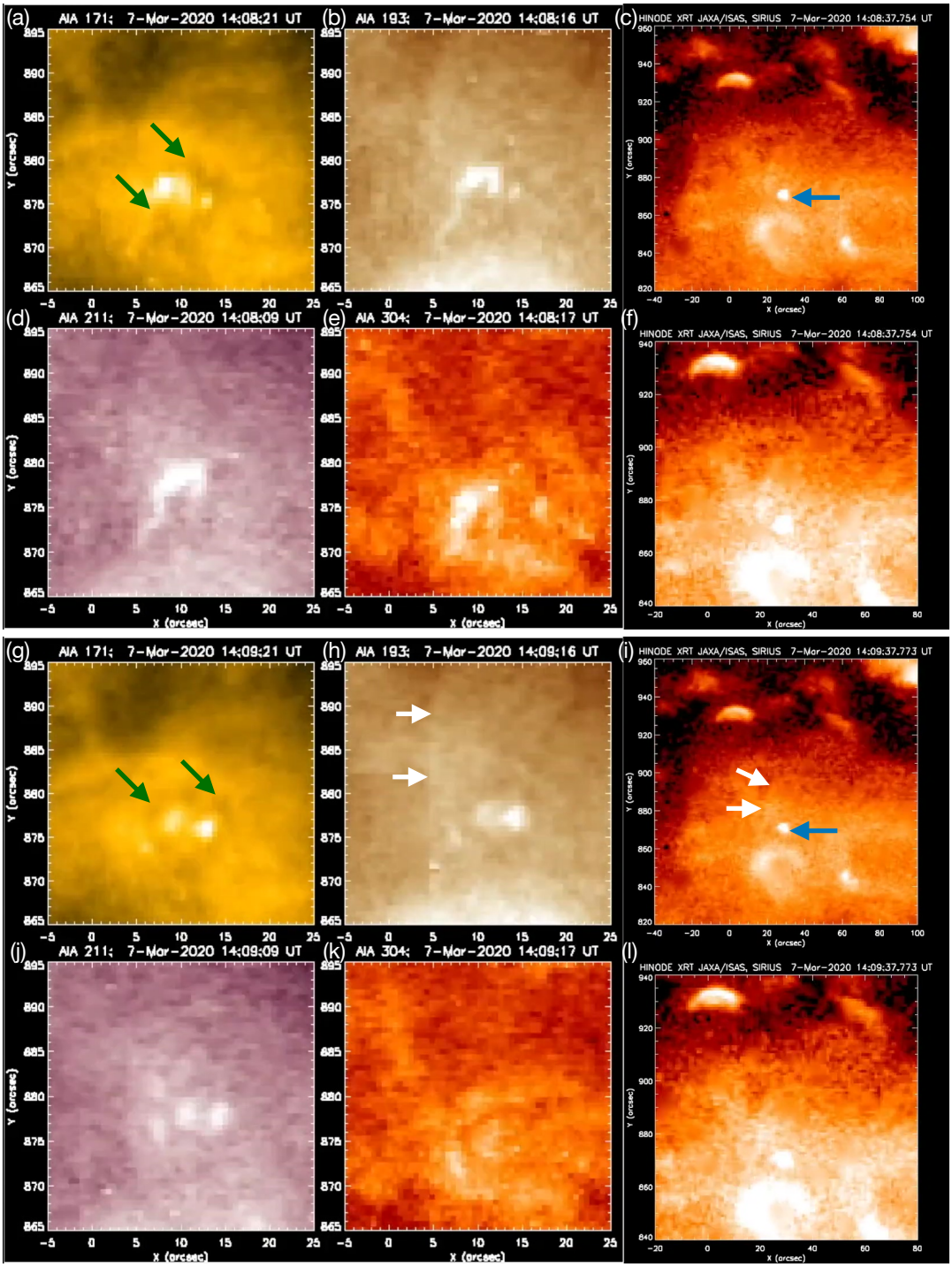

Figure 3. Zoomed-in views of Table 1 event 3, at AIA and XRT wavelengths. Panels (a)—(f) show the region at about the same time, in (a) AIA 171 Å, (b) AIA 193 Å, (c) XRT "thin Al," (d) AIA 211, (e) AIA 304, and (f) XRT thin Al images. The field of view (FOV) is the same for all of the AIA images. For XRT the FOV is larger than that of AIA; both XRT images are at the same time, with panel (f) zoomed-in more than (c), and (f) also uses an intensity scaling set to enhance fainter aspects of the feature. Panels (g)—(l) mimic the ordering and parameters of the images of (a)—(f), but with all of those panels at nearly the same time (within a few seconds of each other), at a later time (about one minute later) than the first six panels. Green arrows show a cool-material erupting minifilament, at two different times in (a) and (g). Blue arrows in (c) and (i) show brightening similar to a coronal-jet jet bright point (JBP). White arrows in (h) and (i) point to a spire that moves away from the JBP location, indicating that the event is likely a faint coronal jet. All of these panels (a—l) are from near the time of the center of the EIS blueshifted contour in Fig. 1, which was at about 14:09 UT (table 1). The accompanying animation shows the evolution of these panels, covering 2020 March 7 over 13:49—14:35 UT. The entire movie runs for 3 s.

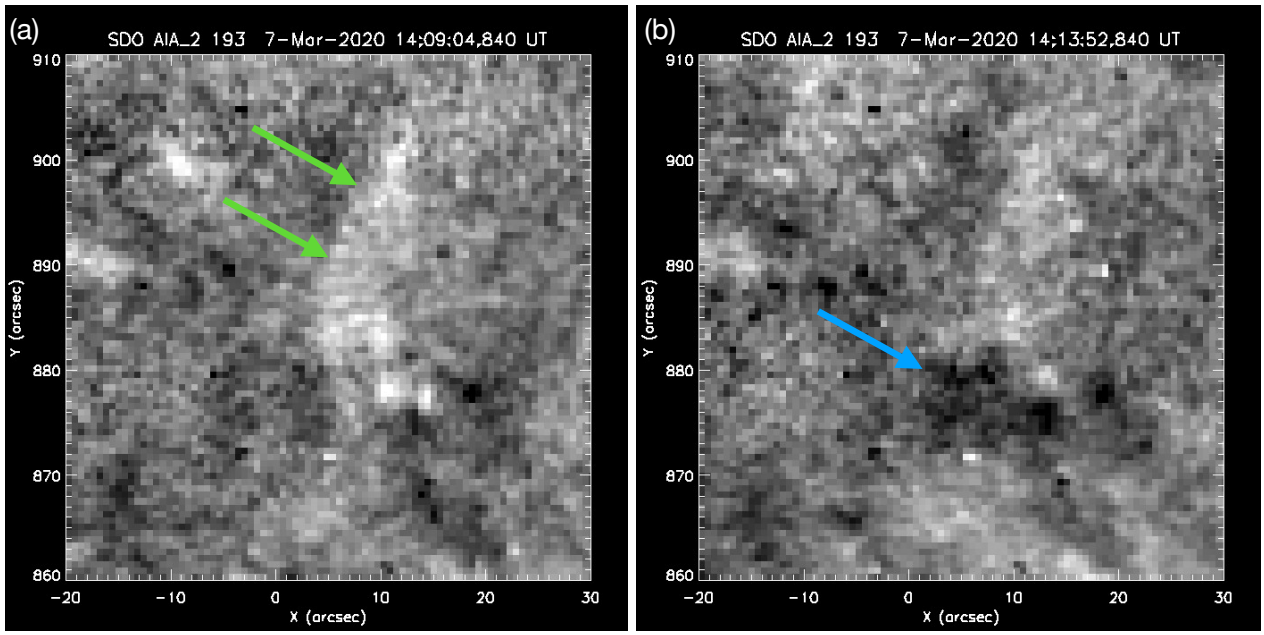

Figure 4. AIA 193 Å difference images of Table 1 event 3. These are fixed differences, whereby we have subtracted the image at 13:49:04 UT in both frames. Panel (a) shows what appears to be a spire of a typical coronal jet (green arrows). Panel (b) shows a dimming region at the base of the apparent spire (blue arrow). The accompanying animation shows the time evolution of difference images, with the same initial frame used here subtracted. The movie covers covering 2020 March 7 over 13:49—14:22 UT, and runs for 3 s.

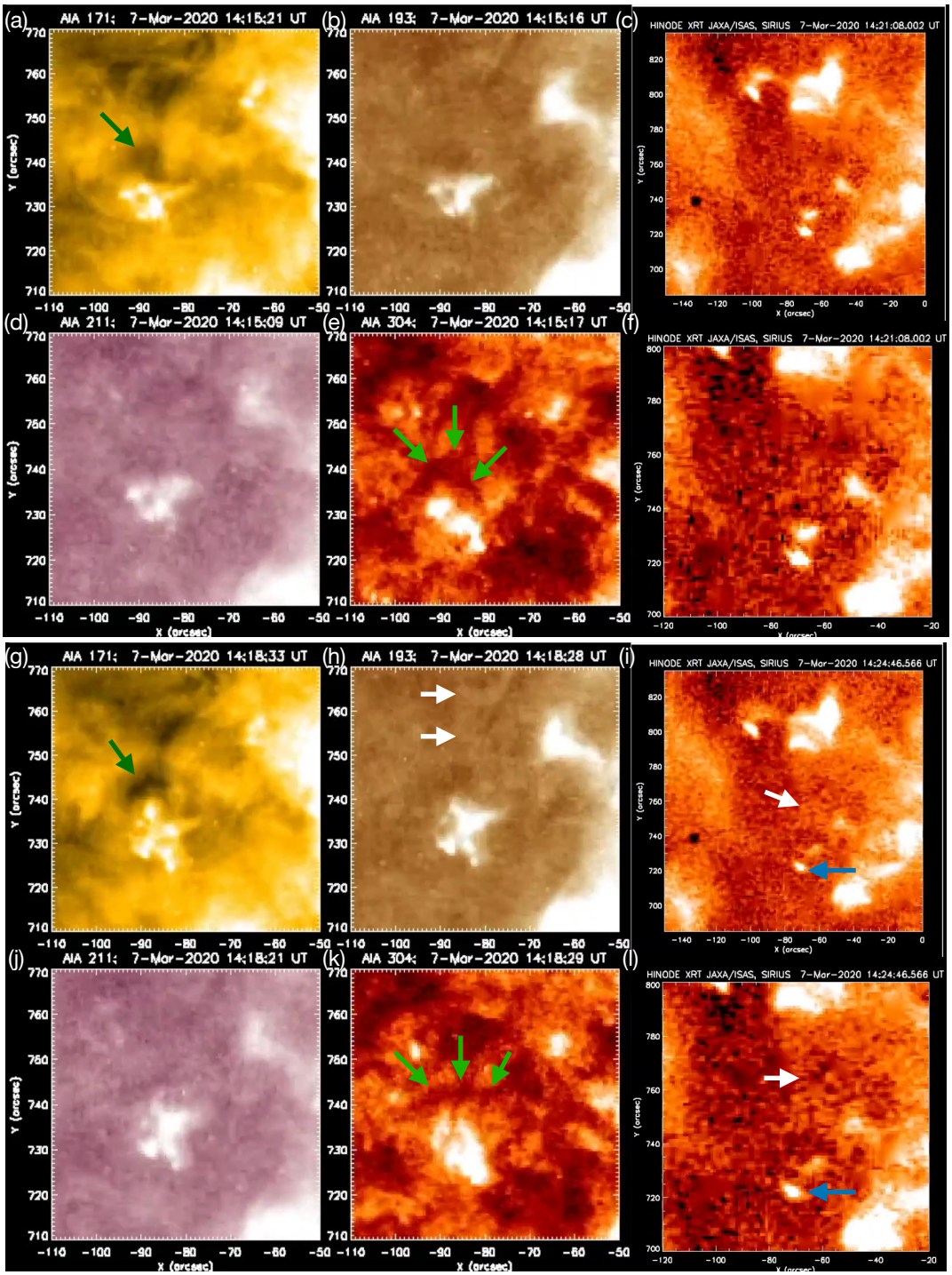

Figure 5. Zoomed-in views of Table 1 event 4, at AIA and XRT wavelengths. The basic layout of the panels is as described in Figure 3. Green arrows show a cool-material erupting minifilament, at about the same time in (a) and (e), and at a later time in (g) and (k). Blue arrows in (i) and (l) show a brightening similar to a JBP. White arrows in (h) and (i) point to a faint feature that resembles a coronal-jet spire. The accompanying animation shows the evolution of these panels, covering 2020 March 7 over 14:00—14:48 UT. The entire movie runs for 3 s. From table 1 the center of the blueshift contour is at about 14:29 UT, at which time the movies still show apparent outflow.

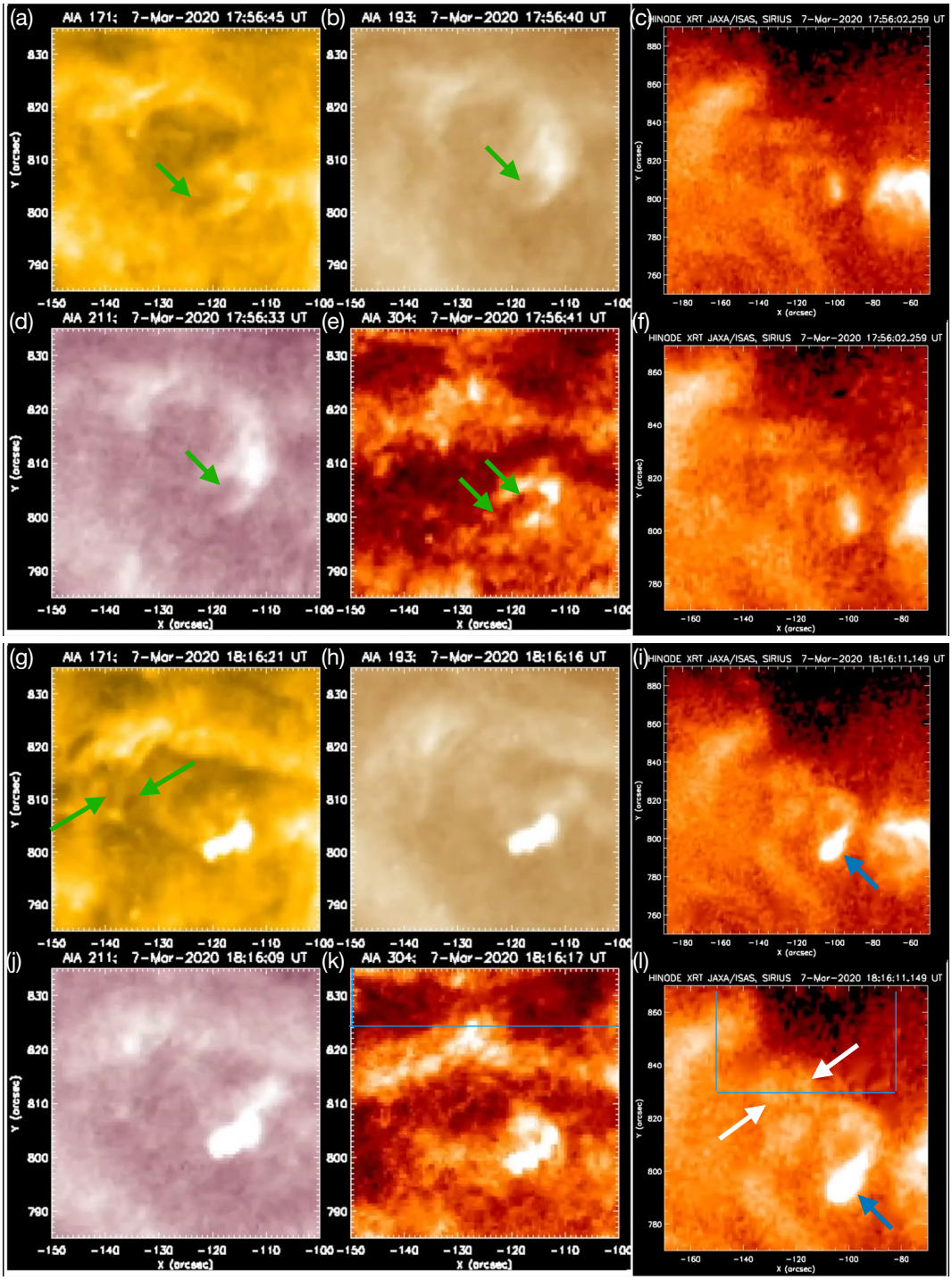

Figure 6. Zoomed-in views of Table 1 event 5, at AIA and XRT wavelengths. The basic layout of the panels is as described in Figure 3. Green arrows show a cool-material erupting minifilament, at about the same time in (a), (b), (d), and (e). Blue arrows in (i) and (l) show a brightening similar to a JBP, and that brightening is visible but saturated in the AIA images in (g), (h), (j), and (k). White arrows in (l) point to either side of a faint feature that resembles a coronal-jet spire. Blue lines in (k) and (l) represent portions of the EIS FOV shown in Fig. 1, and which is shown as a white box in the video accompanying Fig. 2. The animation accompanying the current figure shows the evolution of these panels, covering 2020 March 7 over 17:47—18:44 UT. The animation runs twice, where the first time through an arrow in the 171 Å panel shows outflows from the minifilament-eruption location that reach out to the location near where the spire forms, and the blue lines in the XRT panel represent the FOV of the panel for event 5 in Fig. 1. The second time through the animation plays without the arrow and box overlays. The entire movie runs for 6 s. From table 1 the center of the blueshift contour is at about 18:32 UT, at which time the XRT movie is still consistent with continued outflow.

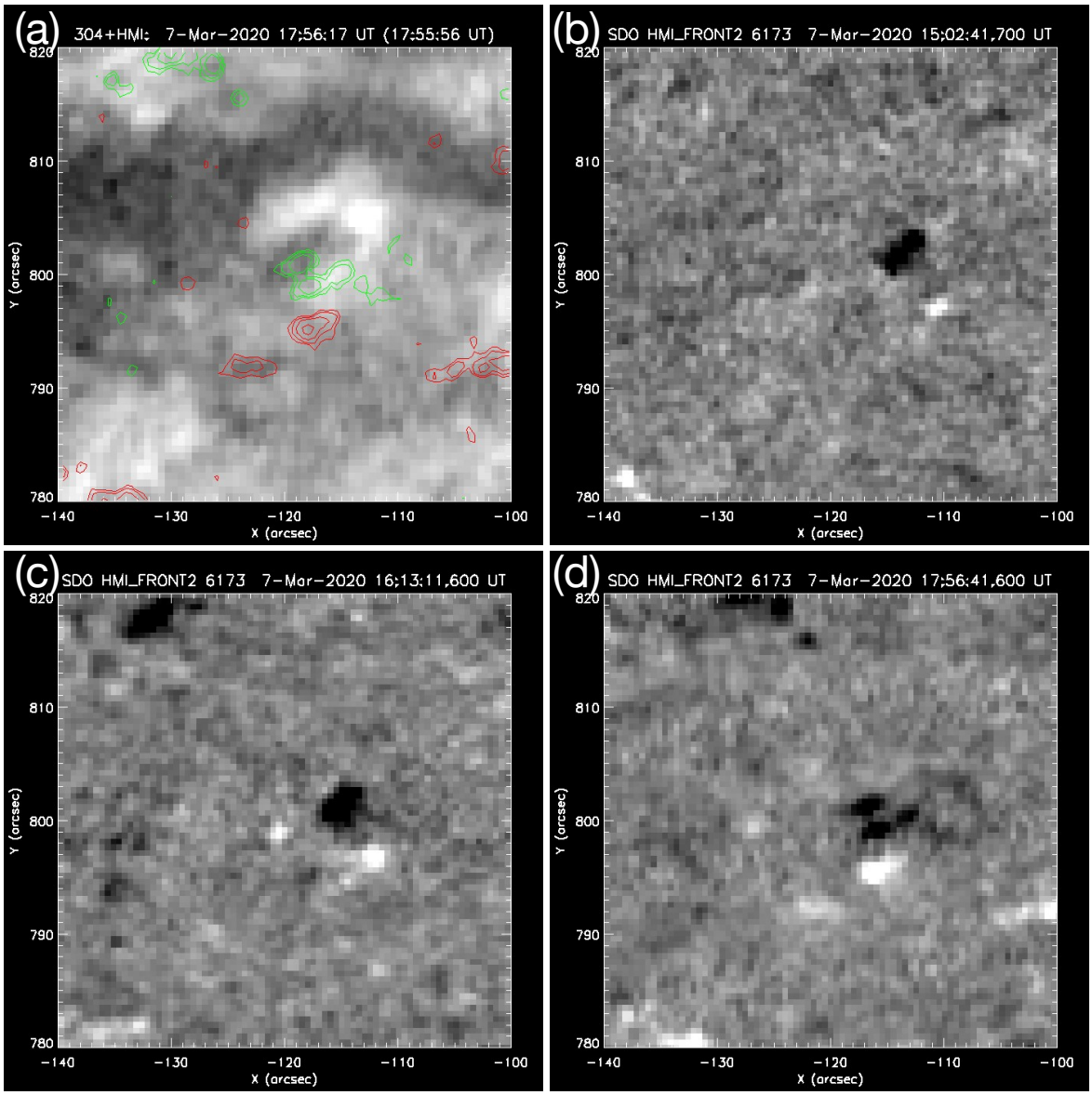

Figure 7. Magnetic field evolution at the base of event 5. Panel (a) shows positive (red) and negative (green) contours from an HMI line-of-sight magnetogram at 17:55:56 UT on 2020 March 2, as contours with levels set at 30 and 50 G. This is overlaid onto a grayscale version of an 304 Å image within seconds of that in Fig. 6(e) (the FOV here is more zoomed in than shown in Fig. 6(e)), just as the minifilament is erupting. That erupting minifilament plausibly formed and was ejected from the neutral line of the two closest opposite-polarity strong flux patches. Panels (b)—(d) show the line-of-sight HMI magnetograms of the location evolving over time, with positive and negative polarities represented by white and black, respectively (contours in (a) are within a minute of (d)). These panels show that the two opposite-polarity patches that may have caused the minifilament eruption converged toward each other in the hours prior to that eruption. Such flux convergence (and cancelation) is commonly observed to occur leading up to minifilament eruptions that produce typical coronal jets. The FOV here is slightly smaller than that of the AIA images in Fig. 6, in order to center the bipolar flux patches better.

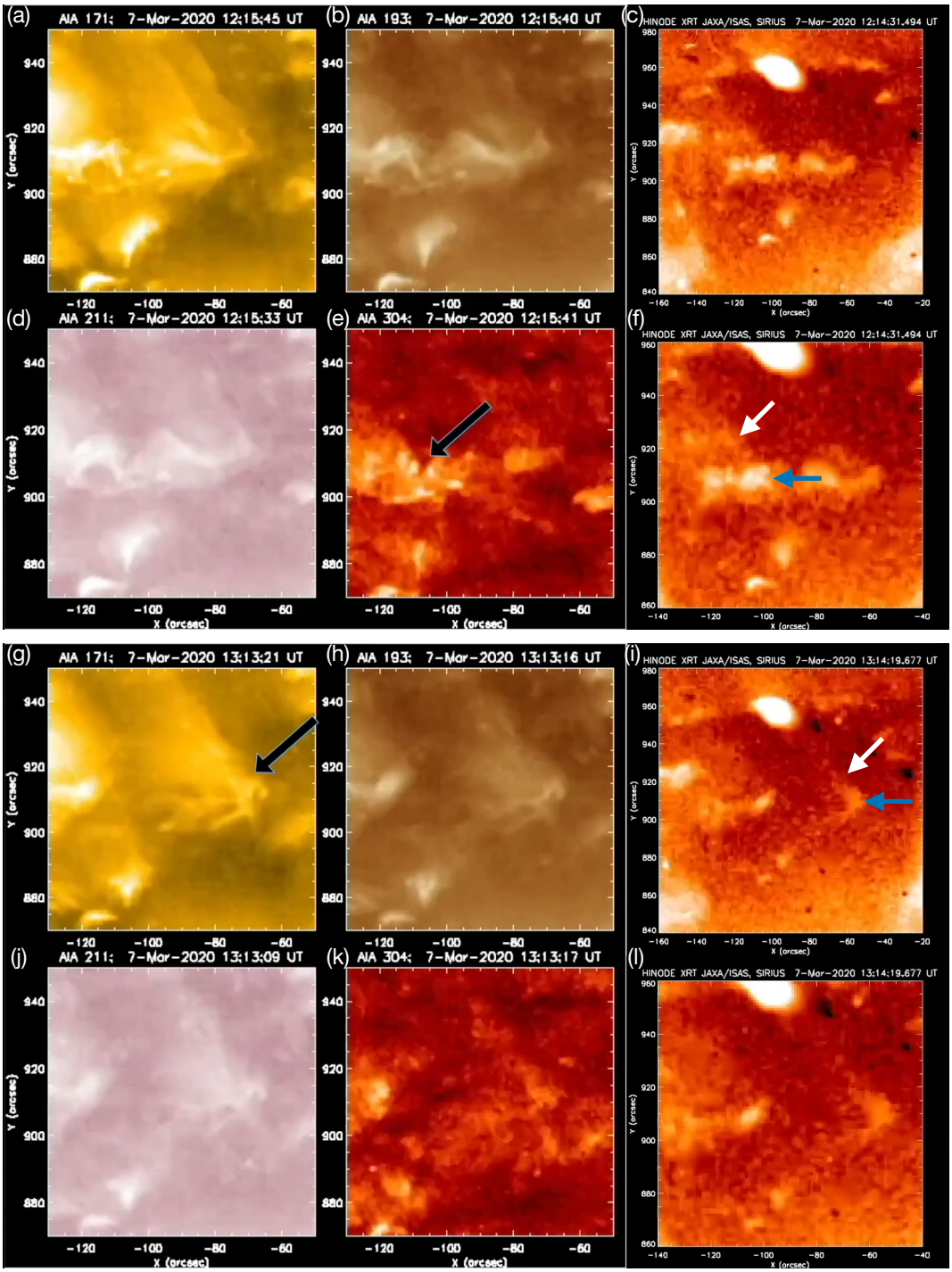

Figure 8. Zoomed-in views of Table 1 event 1 (a—f) and event 2 (g—l), at AIA and XRT wavelengths. The basic layout of the panels is as described in Figure 3. The black arrow in (e) shows a cool-material feature in an AIA 304 Å image that is consistent with being an erupting minifilament, producing the weak jet-spire-like feature pointed to by the white arrow in the XRT frame in panel (f), which feature coincides in time and location with the outflows observed in EIS for event 1. The blue arrow in (f) points to a brightening similar to a JBP adjacent to the spire-like feature. The black arrow in (g) shows a cool-material feature in an AIA 171 Å image that is consistent with being an erupting minifilament, producing the weak jet-spire-like features pointed to in the XRT frame in panel (i), and which coincides in time and location of the outflows observed in EIS for event 2. The blue arrow in (i) points to a brightening similar to a JBP adjacent to the spire-like feature. The accompanying animation shows the evolution of these panels, covering 2020 March 7 over 12:00—13:57 UT. The animation plays twice: the first time through the black arrows of panels (e) and (g) are overlaid, and trace the movement of the cool-material features in time; the second time through the animation plays without any overlays. The entire movie runs for 8 s. From table 1 the center of the blueshift contour for events 1 and 2 are respectively at about 12:18 and 13:19 UT, and the movie shows features consistent with outflows from the respective locations at those times.